

Charge symmetry violation in the determination of strangeness form factors

Ali Alkathiri* and Ross D. Young, James M. Zanotti

CSSM, School of Physical Sciences, University of Adelaide, Adelaide SA 5005, Australia

The strange quark contributions to the electromagnetic form factors of the proton are ideal quantities to study the role of hidden flavor in the properties of the proton. This has motivated intense experimental measurements of these form factors. A major remaining source of systematic uncertainty in these determinations is the assumption that charge symmetry violation (CSV) is negligible. We use recent theoretical determinations of the CSV form factors and reanalyse the available parity-violating electron scattering data, up to $Q^2 \sim 1\text{GeV}^2$. Our analysis considers systematic expansions of the strangeness electric and magnetic form factors of the proton. The results provide an update to the determination of strangeness over a range of Q^2 where, under certain assumptions about the effective axial form factor, an emergence of non-zero strangeness is revealed in the vicinity of $Q^2 \sim 0.6\text{GeV}^2$. Given the recent theoretical calculations, it is found that the current limits on CSV do not have a significant impact on the interpretation of the measurements and hence suggests an opportunity for a next generation of parity-violating measurements to more precisely map the distribution of strange quarks.

I. INTRODUCTION

The desire for a complete understanding of the electromagnetic structure of the proton has led to significant efforts over the last two decades to determine the individual quark flavor contributions to the proton's electromagnetic form factors. A significant challenge in this goal lies in determining the role played by non-valence or “hidden” quark flavors whose contributions arise only through fluctuations of the QCD vacuum. Being the lightest sea-only quark, strange quarks are anticipated to make the most significant contribution. Through an extensive experimental program of parity-violating electron scattering (PVES) [1–12], strange quarks have been tagged by measuring the neutral-current form factors. The isolation of strangeness relies on the assumption of good charge symmetry, which has been one of the limiting factors in extending the experimental program to greater precision. In this work, we quantify the impact of charge symmetry violation (CSV) on the extraction of strangeness from a global analysis of the PVES measurements.

While earlier theoretical predictions of CSV in the proton's electromagnetic form factors varied through several orders of magnitude [13–16], a recent lattice QCD calculation [17] has determined that CSV in the proton's electromagnetic form factors is significantly smaller than earlier expectations. Despite its importance for future measurements of parity violating electron-proton scattering and their subsequent interpretation as evidence of proton strangeness, the precise influence of this recent CSV constraint has not been thoroughly quantified. Hence, here we perform a global analysis of the full existing set of parity-violating (PV) asymmetry data with and without the constraint of CSV form factors. To

achieve this task, we consider PVES data, obtained from experiments conducted with varying kinematics and targets, from SAMPLE [1, 2], PVA4 [3–5], HAPPEX [6–10], G0 [11, 12] and Q_{weak} [18].

This paper is organised as follows: In section II, we describe the formalism of PVES, including PV asymmetries of the nucleon, helium-4 and the deuteron. Section III presents the parametrisation of strange quark form factor, while section IV is dedicated to a study of the CSV effects on strangeness form factor extraction. A brief summary is finally presented in section V.

II. STRANGE FORM FACTORS AND PARITY-VIOLATING ELECTRON SCATTERING

Determining the strange electric and magnetic form factors experimentally requires a process where the weak and electromagnetic interactions interfere. This is achieved through PVES experiments [19, 20], whose leading-order amplitudes are shown in Fig. 1.

Under the assumption of charge symmetry, the PV asymmetry in polarised $e-p$ scattering is given by [21]

$$A_{PV}^p = \left[\frac{-G_F Q^2}{4\sqrt{2}\pi\alpha} \right] (A_V^p + A_s^p + A_A^p). \quad (1)$$

where in terms of the proton's electric ($G_E^{\gamma,p}$) and magnetic ($G_M^{\gamma,p}$) Sach's form factors

$$A_V^p = (1 - 4\sin^2\hat{\theta}_w)(1 + R_V^p) - (1 + R_V^p) \frac{\epsilon G_E^{\gamma,p} G_E^{\gamma,n} + \tau G_M^{\gamma,p} G_M^{\gamma,n}}{\epsilon(G_E^{\gamma,p})^2 + \tau(G_M^{\gamma,p})^2}, \quad (2)$$

$$A_s^p = -(1 + R_V^{(0)}) \frac{\epsilon G_E^{\gamma,p} G_E^s + \tau G_M^{\gamma,p} G_M^s}{\epsilon(G_E^{\gamma,p})^2 + \tau(G_M^{\gamma,p})^2}, \quad (3)$$

and

$$A_A^p = \frac{-\epsilon'(1 - 4\sin^2\hat{\theta}_w)G_M^{\gamma,p}\tilde{G}_A^{e,p}}{\epsilon(G_E^{\gamma,p})^2 + \tau(G_M^{\gamma,p})^2}. \quad (4)$$

* On leave from: Physics Department, Taif University, Taif 26571, Saudi Arabia.

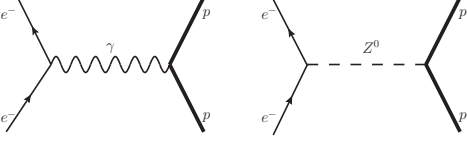


FIG. 1. Total leading order amplitude for electron-nucleon scattering is the sum of the leading order electromagnetic and neutral current amplitudes.

are the proton's vector form factor excluding strangeness (A_V^p), the proton's strangeness vector form factor (A_s^p), and the interference of the proton's magnetic vector and the axial vector form factors (A_A^p).

The electromagnetic form factors of the proton and neutron are denoted by $G_{E,M}^\gamma$, the strangeness vector form factors $G_{E,M}^s$, and the effective axial form factor \tilde{G}_A^p . The kinematic variables, which depend on the four-momentum transfer $Q^2 = -q^2$ and the electron scattering angle θ , are defined as

$$\tau = \frac{Q^2}{4M_p^2}, \quad (5)$$

$$\epsilon = \frac{1}{1 + 2(1 + \tau) \tan^2 \frac{\theta}{2}}, \quad (6)$$

and

$$\epsilon' = \sqrt{\tau(1 + \tau)(1 - \epsilon^2)}, \quad (7)$$

where M_p , ϵ and ϵ' are the proton's mass, the virtual photon longitudinal polarization and the scattered energy, respectively. The standard model parameters: fine structure constant α , Fermi coupling $G_F = 1.16638 \times 10^{-5} \text{ GeV}^2$, the weak mixing angle, $\sin^2 \hat{\theta}_W = 0.23129$, in the $\overline{\text{MS}}$ renormalization scheme, and the standard model radiative corrections, $R_V^p = -0.0513$ and $R_V^n = R_V^{(0)} = -0.0098$ are all obtained from the PDG [22].

A. Helium-4 and Deuteron PV Asymmetries

The ^4He nucleus is spin zero, parity even and isoscalar. Elastic electron scattering from ^4He is an isoscalar $0^+ \rightarrow 0^+$ transition and therefore allows no contributions from magnetic or axial-vector currents. Thus, the HAPPEX Collaboration has utilised a ^4He target to directly extract the strange electric form factor [6]. Nuclear corrections are relevant for ^4He and deuteron targets, more details about which can be found in [23, 24].

The theoretical asymmetry based on the assumption

that isospin mixing can be neglected is written as [21]

$$A_{PV}^{He} = \left[\frac{G_F Q^2}{4\sqrt{2}\pi\alpha} \right] \cdot \left[(1 - 4\sin^2 \theta_w)(1 + R_V^p) - (1 + R_V^n) \right. \\ \left. + 2 \frac{-(1 + R_V^{(0)})G_E^s}{G_E^p + G_E^n} \right]. \quad (8)$$

Corrections associated with isospin violations will be considered in Section IV.

The parity-violating asymmetries measured in quasi-elastic scattering from the deuteron have responses which involve the deuteron wavefunctions. For this analysis, we use directly the theoretical asymmetries as reported with original experimental measurements. Early results from SAMPLE have had minor modifications made to update for more recent radiative corrections and form factor parameterisations, as described in Ref. [25].

B. γZ -exchange corrections to PVES

Leading electroweak corrections play a significant role in precision measurements of the strangeness contribution to the nucleon form factors [21, 26]. In contrast to the formalism relevant to atomic parity violation experiments [27], an energy-dependent correction arising from the γZ box diagram was highlighted by Gorchtein & Horowitz [28]. The size of this correction is particularly significant to the standard model test by the Q-weak Experiment [29]. Fortunately, the uncertainties arising from the underlying γZ interference structure functions can be reliably constrained [30]. These results have been further supported by direct measurement [31].

The significance of the γZ box is somewhat less pronounced in the determination of strangeness. Nevertheless, for example, the correction makes about $\sim \frac{1}{2}$ -sigma shift to the central value of the precise HAPPEX proton point at $Q^2 \sim 0.1 \text{ GeV}^2$. We incorporate the corrections reported by the constrained model of Ref. [30], updated with the improved constraints of quark-hadron duality [32], and a momentum dependence as proposed in Ref. [33]. For completeness, a table of values is included in Appendix B.

C. Theoretical asymmetries

In this work, a set of all available PV asymmetry data up to $Q^2 \sim 1 \text{ GeV}^2$, as summarised in Table III, is analysed. Such a combined analysis of the world PV data requires a consistent treatment of the vector and axial form factors and radiative corrections. The theoretical asymmetry used in this analysis is written as

$$A_{Theory} = \eta_0 + \eta_A^p \tilde{G}_A^p + \eta_A^n \tilde{G}_A^n + \eta_E G_E^s + \eta_M G_M^s, \quad (9)$$

where the η 's, provided in Table III, are calculated using the recent elastic form factor parameterisations of Ye et al. [34] and current values for the standard model radiative corrections [22].

In this analysis, since the entire contribution is to be fit to data, we employ the effective axial form factors $\tilde{G}_A^{p,n}$ which implicitly includes both the axial radiative and anapole corrections. For these form factors, we employ a dipole form

$$\tilde{G}_A^{p,n} = \tilde{g}_A^{p,n} \left(1 + \frac{Q^2}{M_A^2} \right)^{-2}, \quad (10)$$

with an axial dipole mass $M_A = 1.026$ GeV, determined from neutrino scattering [35], common to both proton and neutron form factors. The normalisations $\tilde{g}_A^{p,n}$ are fit to the data, however since the isoscalar combination is very poorly determined, we choose to impose theoretical estimates based on an effective field theory (EFT) with vector-meson dominance (VMD) model to constrain this combination, $(\tilde{g}_A^p + \tilde{g}_A^n)/2 = -0.08 \pm 0.26$ [36].

III. ANALYSIS FRAMEWORK

A. Taylor expansion

At low momentum transfers, a Taylor series expansion of the electromagnetic form factors in Q^2 is sufficient and minimises the model dependence. Given the sparsity and precision of the available data—up to $\sim 1 \text{ GeV}^2$ —we avoid introducing a specific model by first attempting to parameterise the strange electric and magnetic form factors Q^2 dependence by

$$\begin{aligned} G_E^s &= \rho_s Q^2 + \rho'_s Q^4, \\ G_M^s &= \mu_s + \mu'_s Q^2. \end{aligned} \quad (11)$$

B. z -expansion

A priori, one might not expect a Taylor expansion up to $\sim 1 \text{ GeV}^2$ to be satisfactory. To provide an alternative functional form to the Taylor expansion, we also consider the z -expansion which offers improved convergence based on the analytic properties of the form factors [37–39]. We describe the momentum dependence of the strange form factors using the z -expansion, also to second (nontrivial) order:

$$\begin{aligned} G_E^s &= \rho_{s,z} z + \rho'_{s,z} z^2, \\ G_M^s &= \mu_s + \mu'_{s,z} z, \end{aligned} \quad (12)$$

where

$$z = \frac{\sqrt{t_{cut} + Q^2} - \sqrt{t_{cut}}}{\sqrt{t_{cut} + Q^2} + \sqrt{t_{cut}}}. \quad (13)$$

In our fits, we use choose $t_{cut} = (2m_K)^2$, with the kaon mass $m_K = 0.494$ GeV. In the absence of isospin violation, the cut formally starts at $9m_\pi^2$, but we assume that the strangeness contribution to the 3-pion state can be neglected. We note that, with the current experimental precision, there isn't any significant sensitivity to the value of t_{cut} . To more easily facilitate the comparison with the two expansion forms, we report the simple Taylor expansion coefficients for each case. That is, for the z fits, we translate the expansions back in the leading Taylor form, e.g. $\rho_s = dG_E^s/dQ^2|_{Q^2=0}$.

C. Charge symmetric results

Here we summarise the fit results under the assumption of exact charge symmetry. This provides a baseline with which to explore the implications of charge symmetry violation in the following section.

In this work we perform a global fit at leading order (LO) and at next leading order (NLO) of the strangeness form factor. Thus, the fitting procedure at LO considers four parameters, \tilde{g}_A^p , \tilde{g}_A^n , μ_s and ρ_s , while fitting at NLO considers an additional two parameters, μ'_s and ρ'_s .

The χ^2 is calculated as

$$\chi^2 = \sum_i \sum_j (m_i - t_i)(V)_{ij}^{-1}(m_j - t_j), \quad (14)$$

where m and t denote the measurement and theory asymmetry respectively. The indices i and j run over the data ensemble. The matrix V represents the covariance error matrix defined as

$$(V)_{ij} = (\sigma_i^{uncor})^2 \delta_{ij} + \sigma_i^{cor} \sigma_j^{cor}, \quad (15)$$

where σ_i^{uncor} and σ_i^{cor} are uncorrelated and correlated uncertainties of the i^{th} -measurement, respectively. We note that the correlated uncertainties are only relevant for the G0 experiment, where the forward [11] and backward [12] are treated as mutually independent. The goodness of fit is estimated from the reduced χ^2 as

$$\chi_{red}^2 = \chi^2/\text{d.o.f}, \quad (16)$$

with 33 and 31 degrees of freedom (d.o.f) for the LO and NLO fits, respectively. Note that with the isoscalar axial “charge” constrained, as described above, there are effectively 3(5) fit parameters in the LO(NLO) fits.

We report the leading-order fit results in Table I, with comparisons against previous work. The results are compatible with earlier work, though with significantly reduced uncertainty. This is due to both an updated list of measurements and the inclusion of the full range of Q^2 points in the fit. No appreciable difference is seen between the simple Taylor expansion and the z -expansion.

While the fit quality is reasonable, these simple leading-order fits are certainly anticipated to be too simple to describe these form factors over the full range

TABLE I. The parameter values and χ^2 obtained from previous PVES global fits [25, 40–42] and the current global analysis at LO for both Taylor and z -expansion form factor fits without constraints from CSV.

	ρ_s [GeV $^{-2}$]	μ_s	χ^2_{red}
YRCT(2006) [25]	-0.06 ± 0.41	0.12 ± 0.55	1.3
YRCT(2007) [41]	0.02 ± 0.18	-0.01 ± 0.25	—
LMR(2007) [42]	-0.08 ± 0.16	0.29 ± 0.21	1.3
GCD(2014) [40]	0.26 ± 0.16	-0.26 ± 0.26	1.3
Taylor	0.15 ± 0.04	-0.12 ± 0.04	1.1
z -exp.	0.18 ± 0.05	-0.10 ± 0.04	1.1

TABLE II. The NLO parameters values and χ^2 obtained from a previous global fit [25], where $Q^2 < 0.3$ GeV 2 , and the current global analysis at NLO for both Taylor and z -expansion form factor fits without constraints from CSV.

	ρ_s [GeV $^{-2}$]	ρ'_s [GeV $^{-4}$]	μ_s	μ'_s [GeV $^{-2}$]	χ^2_{red}
YRCT(2006) [25]	-0.03 ± 0.63	-1.5 ± 5.8	0.37 ± 0.79	0.7 ± 6.8	1.4
Taylor	0.07 ± 0.14	0.14 ± 0.22	-0.05 ± 0.15	-0.11 ± 0.23	1.23
z -exp.	0.08 ± 0.17	0.19 ± 0.37	-0.09 ± 0.14	-0.06 ± 0.29	1.26

$0 \leq Q^2 \lesssim 1.0$ GeV 2 . As a result, the statistical uncertainties displayed are not representative of the current knowledge of the strange form factors. We hence allow for more variation in the Q^2 dependence by extending the fits to next-leading order, Eqs. (11) and (12). Results are shown in Table II. Curiously the additional fit parameters are unable to make significant improvement to the χ^2 and the reduced χ^2 very marginally increases for the NLO fit.

Although the data do not support any structure offered by the NLO fits, we prefer the results at this order as being better representative of the uncertainties of the strangeness form factors, while offering some degree of smoothing of the underlying data. We note that given the clustering of the underlying data set, the separation of the electric and magnetic strange form factors are only most reliable at the discrete momentum transfers near $Q^2 \sim 0.1, 0.2$ and 0.6 GeV 2 . As such, the NLO fits are roughly fitting 3 data points with 2 parameters for each form factor. Attempting further higher order will just amount to over-fitting the statistical fluctuations of the data set.

The comparison between the leading and next-to-leading order fits for the Taylor expansion are shown in Figure 2. The corresponding z -expansion results are very similar. In Fig. 3 we show the NLO z -expansion parameterisation of the separated electric and magnetic form factors and compare with recent lattice QCD results [43, 44]. Here we observe excellent agreement between our strangeness determination based on PVES data and lattice QCD results over the full Q^2 range. These are also compatible with earlier lattice [45] and lattice-constrained [46–48] results. Interestingly, we note that the experimental results are showing some support for a non-vanishing strangeness electric form factor in the vicinity of $Q^2 \sim 0.6$ GeV 2 . Given the lack of sensitivity to the choice of functional form, we adopt the z -expansion

at NLO as our preferred fit for the following discussions.

The preceding discussion has focussed on the separation of the electric and magnetic strangeness form factors. Given the high degree of correlation in the measurements, it is instructive to display the joint confidence intervals. Fig. 4 displays the 95% confidence level ellipses for the different values of $Q^2 = 0.1, 0.23$ and 0.63 GeV 2 for the NLO z -expansion fit. At the low Q^2 values, we observe that the strangeness form factors are compatible with zero at the 95% CL, with a marginal preference for positive values of strange electric form factor and negative values of the magnetisation — as seen earlier in Refs. [41, 49].

At $Q^2 = 0.63$ GeV 2 , there appears a clear signal for nonzero strangeness, with a negative G_M^s and positive G_E^s . In contrast to earlier work that has suggested vanishing strangeness at this Q^2 [10, 12], the dominant difference in the present work is the treatment of the axial/anapole form factor. As described, the isoscalar combination is constrained by the EFT and VMD estimate of Zhu et al. [36], while the isovector combination is determined by the data. The best fit—for z -expansion at NLO—results in $\tilde{g}_A^p = -0.67 \pm 0.25$, which is less negative than the zero-anapole approximation. As a consequence, the data-driven fit drives the back-angle G0 results to be more consistent with a negative G_M^s . Under these assumptions for the effective axial form factor, we see $G_E^s \sim 0.1$, which—with the strange charge factor included—is on the order of 10% of the proton electric form factor at this momentum transfer. Given the smallness of the strange form factors determined in direct lattice calculations [44, 45], the result seen here suggests a future investigation of the anapole “charge” and Q^2 dependence is warranted.

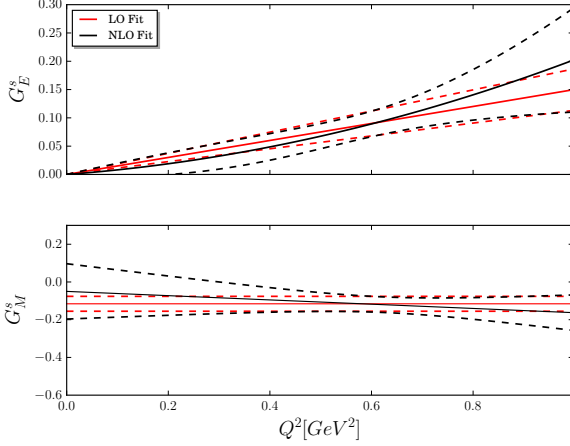


FIG. 2. The extracted strange electric and magnetic form factors from a global fit up to $Q^2 \sim 1 \text{ GeV}^2$ using the Taylor expansions in Eq. (11). The red (black) solid curve shows the LO (NLO) fit and bound shown by the dotted curves.

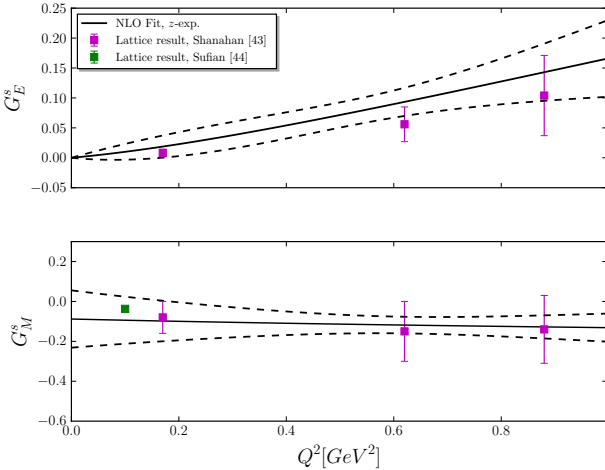


FIG. 3. The extracted strange electric and magnetic form factors from global fit up to $Q^2 \sim 1 \text{ GeV}^2$ with using the NLO z -expansion in Eq. (12). A comparison with recent lattice QCD results is shown where the green square (errors bars smaller than the symbol) corresponds to the result of $G_M^s(Q^2 = 0.1 \text{ GeV}^2)$ [44] and the magenta squares are G_M^s and G_E^s at $Q^2 = 0.17, 0.62$ and 0.88 GeV^2 [43].

IV. SENSITIVITY TO CHARGE SYMMETRY VIOLATION

A. CSV in asymmetries

In this section we study the effects of charge symmetry violation on our results, i.e. we no longer have a relationship between the individual quark flavour contributions

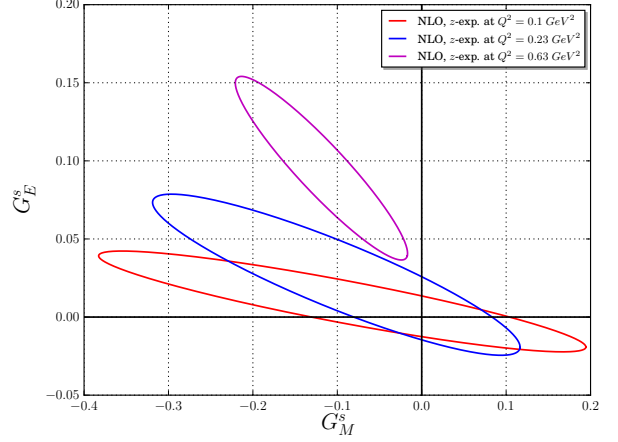


FIG. 4. 95% confidence level ellipses for the electric and magnetic strangeness form factors using the NLO z -expansion in Eq. (12) for three Q^2 values 0.1, 0.23, 0.63 GeV^2 .

to the proton and neutron form factors

$$G_{E,M}^{p,u} \neq G_{E,M}^{n,d},$$

$$G_{E,M}^{p,d} \neq G_{E,M}^{n,u}.$$

We follow standard notation and define the CSV form factors as

$$G_{E,M}^{CSV} = \frac{2}{3}(G_{E,M}^{p,d} - G_{E,M}^{n,u}) - \frac{1}{3}(G_{E,M}^{p,u} - G_{E,M}^{n,d}). \quad (17)$$

In order to explore the impact of CSV, we need to modify the neutral weak form factors to explicitly include a CSV term

$$G_{E,M}^{Z,p} = (1 - 4 \sin^2 \hat{\theta}_W)(1 + R_V^p)G_{E,M}^{\gamma,p} - (1 + R_V^n)G_{E,M}^{\gamma,n} - (1 + R_V^{(0)})G_{E,M}^s - (1 + R_V^n)G_{E,M}^{CSV}, \quad (18)$$

where the Q^2 -dependence of each form factor has been dropped for clarity. The CSV form factor can be expressed as a simple Taylor expansion in Q^2

$$G_{E,M}^{CSV}(Q^2) = G_{E,M}^{CSV}(0) - \rho_{E,M}^{CSV} Q^2 + \mathcal{O}(Q^4), \quad (19)$$

with $G_{E,M}^{CSV}$ set to zero at $Q^2 = 0$ due to charge conservation.

Regarding the theoretical asymmetry given in Eq. 9, we note that η_0 will receive a correction due to the CSV form factor. Hence

$$A_{Theory} = \eta_0^{CSV} + \eta_A^p \tilde{G}_A^p + \eta_A^n \tilde{G}_A^n + \eta_E G_E^s + \eta_M G_M^s, \quad (20)$$

where $\eta_0^{CSV} = \eta_0 + \eta_E^{CSV} G_E^{CSV} + \eta_M^{CSV} G_M^{CSV}$, with

$$\eta_{CSV,E}^N = \left[\frac{G_F Q^2}{4\sqrt{2}\pi\alpha} \right] \cdot \left[\frac{(1 + R_V^n)\epsilon G_E^{\gamma,N}}{\epsilon(G_E^{\gamma,N})^2 + \tau(G_M^{\gamma,N})^2} \right], \quad (21)$$

$$\eta_{CSV,M}^N = \left[\frac{G_F Q^2}{4\sqrt{2}\pi\alpha} \right] \cdot \left[\frac{(1 + R_V^n)\tau G_M^{\gamma,N}}{\epsilon(G_E^{\gamma,N})^2 + \tau(G_M^{\gamma,N})^2} \right]. \quad (22)$$

In the case of the PV asymmetry of ^4He , we should consider nuclear CSV, which we denote F^{CSV} , in addition to CSV at nucleon level, G_E^{CSV} . In this case, η_0^{CSV} can therefore be written as

$$\eta_0^{CSV} = \eta_0 - 2F^{CSV} + 4 \frac{(1 + R_V^n) G_E^{CSV}}{G_E^p + G_E^n}, \quad (23)$$

where in the notation of [50], $F^{CSV} \equiv F^{(1)}(q)/F^{(0)}(q) = -0.00157$ is used to calculate η_0^{CSV} for the theoretical PV asymmetry of ^4He at $Q^2 = 0.077$ and 0.091 GeV^2 .

B. CSV Theoretical Works

To include effects of charge symmetry violation in our determination of the strangeness form factors, we consider three different calculations of the CSV form factors. The first work we consider is from Kubis and Lewis [13], denoted by “K&L CSV”. They used effective field theory, supplemented with resonance saturation to estimate the relevant contact term — where the CSV is largely driven by ρ – ω mixing. To accomplish this, they employ a large ω -nucleon coupling constant $g_\omega \sim 42$ taken from dispersion analysis. Combining this estimate with calculations in HB χ PT and infrared regularised baryon chiral perturbation theory, K&L predicted a CSV magnetic moment contribution $G_M^{CSV}(0) \equiv k^{u,d} = 0.025 \pm 0.020$, which includes an uncertainty arising from the resonance parameter. For the CSV slope parameters, K&L found $\rho_M^{CSV} = -0.08 \pm 0.06 \text{ GeV}^{-2}$ and $\rho_E^{CSV} = -0.055 \pm 0.015 \text{ GeV}^{-2}$. We take these values as our first estimate of the CSV form factors.

The second theoretical calculation of CSV we consider is from Wagman and Miller [14], denoted by “W&M CSV”. In their work, they used relativistic chiral perturbation theory with a more realistic ω -nucleon coupling i.e. $g_\omega \sim 10$. That study reported values of $G_M^{CSV}(0) = 0.012 \pm 0.003$, $\rho_M^{CSV} = 0.015 \pm 0.010 \text{ GeV}^{-2}$ and $\rho_E^{CSV} = -0.018 \pm 0.003 \text{ GeV}^{-2}$.

The third determination of the CSV form factor that we employ is based on an analysis of lattice QCD results [17], that we refer to as “Lattice CSV”. The lattice study found significantly smaller values of the magnetic and electric CSV form factors compared to the previous two estimates. To study the effect of the CSV form factors obtained from lattice QCD, we summarise the results of Ref. [17] by $G_M^{CSV} = 0.0 \pm 0.001$ and $\rho_E^{CSV} = 0.0 \pm 0.001 \text{ GeV}^{-2}$.

C. Strangeness with CSV

In order to propagate the uncertainties, we extend the covariance matrix above, Eq. (15), to include a correlated

uncertainty associated with the theoretical estimates of CSV. For each theoretical description, we reanalyse the entire data set and present in Fig. 5 our determination of the strange magnetic moment μ_s (left) and strange electric radius ρ_s (right). Since the Lattice CSV form factors are zero with a negligible uncertainty, they are consistent with the “No CSV” results. We also find no visible impact on μ_s and ρ_s from the inclusion of the W&M CSV form factors. Finally, when estimating the CSV form factors by the K&L parameters, we observe only small shifts in the central value of the strangeness magnetic moment. Nevertheless, even the “worst case” scenario of K&L doesn’t appreciably affect the NLO fits.

V. CONCLUSION

We have presented a complete global analysis of all PVES asymmetry data for the proton, ^4He and deuterium. We have investigated the γZ exchange correction and the effect that CSV form factors have on the extraction of strange quark contribution. Including γZ box contribution in the analysis leads to small increases in the magnitude of the central values of μ_s and ρ_s when compared to results obtained without constraints from γZ -exchange. CSV results considered in this work have tiny effects on the central values of the strangeness parameters, with the largest effect, while still small, coming from the inclusion of CSV form factors as provided by Kubis and Lewis [13]. Our results favour non-zero values for the strangeness magnetic moment and electric radius, with the most significant constraints coming from the LO fits using a Taylor expansion for the strangeness form factors. Finally, in order to examine the model dependence of employing a Taylor expansion in our analysis, we also included fits using the z -expansion which were found to be in agreement.

The latest theory estimates on CSV are small — indeed small enough that they would not cloud the interpretation of future precision strangeness measurements. However, we note that the back-angle measurements do exhibit sensitivity to the effective axial form factor, presenting an opportunity for future investigation. The combined efforts to improve the resolution of strangeness, and reveal the structure of the anapole form factor offer the potential to establish a precision era of QCD and the nucleon. While further advancing the understanding of the mechanisms underlying nonperturbative QCD, such work will serve to gain further confidence in the use of lattice QCD for precision constraints in tests of the standard model.

ACKNOWLEDGMENTS

We would like to thank Wally Melnitchouk for useful discussions. AA is supported by Physics Department, Taif University. RDY and JMZ are supported by the

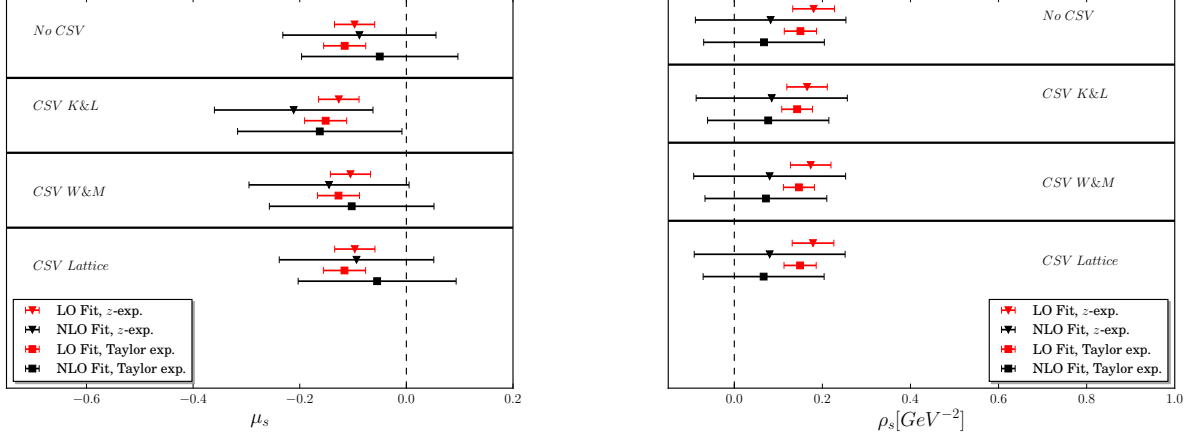


FIG. 5. Comparison of determinations obtained from the present work with and without CSV for the strange magnetic moment μ_s (left) and strange electric radius ρ_s (right).

Australian Research Council under grants FT120100821, FT100100005, DP140103067 and DP190100297.

Appendix A: Parity violating asymmetries

Table III lists the asymmetries and their dependence on the leading unknown hadronic structure for all existing PVES experiments.

Appendix B: Energy dependence of the γ -Z box

To incorporate the effect induced by the energy-dependent component of the γ -Z box radiative correction, the measured PV asymmetries given in Eq. (1) are modified by

$$A_{PV\,corr}^p = A_{PV}^p - \left[\frac{-G_F Q^2}{4\sqrt{2}\pi\alpha} \right] \square_{\gamma Z}(E, Q^2). \quad (B1)$$

The forward (or vanishing momentum transfer) limit of this box are taken from Ref. [32], which extends Ref. [30] to also incorporate duality constraints. To estimate the momentum transfer dependence, we adopt the model suggested by Gorchtein *et al.* [33]:

$$\square_{\gamma Z}(E, Q^2) = \square_{\gamma Z}(E, 0) \frac{\exp(-BQ^2/2)}{F_1^p(Q^2)}, \quad (B2)$$

with slope parameter estimated to be $B = 7 \pm 1 \text{ GeV}^2$, and F_1^p the electromagnetic Dirac form factor of the proton. The numerical values used in this work are summarised in Table IV.

-
- [1] E. J. Beise, M. L. Pitt, and D. T. Spayde, Prog. Part. Nucl. Phys. **54**, 289 (2005), arXiv:nucl-ex/0412054 [nucl-ex].
 - [2] D. T. Spayde *et al.* (SAMPLE), Phys. Lett. **B583**, 79 (2004), arXiv:nucl-ex/0312016 [nucl-ex].
 - [3] F. E. Maas *et al.* (A4), Phys. Rev. Lett. **93**, 022002 (2004), arXiv:nucl-ex/0401019 [nucl-ex].
 - [4] S. Baunack *et al.*, Phys. Rev. Lett. **102**, 151803 (2009), arXiv:0903.2733 [nucl-ex].
 - [5] F. E. Maas *et al.*, Phys. Rev. Lett. **94**, 152001 (2005), arXiv:nucl-ex/0412030 [nucl-ex].
 - [6] K. A. Aniol *et al.* (HAPPEX), Phys. Rev. Lett. **96**, 022003 (2006), arXiv:nucl-ex/0506010 [nucl-ex].
 - [7] K. A. Aniol *et al.* (HAPPEX), Phys. Rev. **C69**, 065501 (2004), arXiv:nucl-ex/0402004 [nucl-ex].
 - [8] K. A. Aniol *et al.* (HAPPEX), Phys. Lett. **B635**, 275 (2006), arXiv:nucl-ex/0506011 [nucl-ex].
 - [9] A. Acha *et al.* (HAPPEX), Phys. Rev. Lett. **98**, 032301 (2007), arXiv:nucl-ex/0609002 [nucl-ex].
 - [10] Z. Ahmed *et al.* (HAPPEX), Phys. Rev. Lett. **108**, 102001 (2012), arXiv:1107.0913 [nucl-ex].
 - [11] D. S. Armstrong *et al.* (G0), Phys. Rev. Lett. **95**, 092001 (2005), arXiv:nucl-ex/0506021 [nucl-ex].
 - [12] D. Androic *et al.* (G0), Phys. Rev. Lett. **104**, 012001 (2010), arXiv:0909.5107 [nucl-ex].
 - [13] B. Kubis and R. Lewis, Phys. Rev. **C74**, 015204 (2006), arXiv:nucl-th/0605006 [nucl-th].
 - [14] M. Wagman and G. A. Miller, Phys. Rev. **C89**, 065206 (2014), [Erratum: Phys. Rev. **C91**, no.1, 019903(2015)], arXiv:1402.7169 [nucl-th].

TABLE III. Values of η_i , appearing in Eq. 9, which describe the theoretical asymmetry for each experiment (in parts-per-million). A^{phys} and δA are the measured asymmetry and the corresponding uncertainty respectively where the statistic and systematic error have been added in quadrature. While δA_{cor} is the correlated error in the G0 experiment [11, 12].

Experiment	Target	Q^2	θ	E	η_0	η_A^p	η_A^n	η_E	η_M	A^{phys}	δA	δA_{cor}	Ref.
SAMPLE	d	0.038	144	0.11	-2.13	0.46	-0.30	1.16	0.28	-3.51	0.81	0	[1]
SAMPLE	d	0.091	144	0.18	-7.02	1.04	-0.65	1.63	0.77	-7.77	1.03	0	[1]
SAMPLE	p	0.1	144	0.2	-5.50	1.57	0	2.11	3.45	-5.61	1.11	0	[2]
HAPPEX	p	0.477	12.3	3.35	-15.82	1.13	0	55.65	23	-15.05	1.13	0	[7]
PVA4	p	0.230	35.3	0.85	-5.78	0.88	0	22.45	5.08	-5.44	0.60	0	[3]
PVA4	p	0.108	35.4	0.57	-1.82	0.26	0	10.07	1.05	-1.36	0.32	0	[5]
G0	p	0.122	6.68	3.03	-1.93	0.06	0	11.94	1.17	-1.51	0.49	0.18	[11]
G0	p	0.128	6.84	3.03	-2.08	0.06	0	12.58	1.30	-0.97	0.46	0.17	[11]
G0	p	0.136	7.06	3.03	-2.28	0.07	0	13.43	1.47	-1.30	0.45	0.17	[11]
G0	p	0.144	7.27	3.03	-2.48	0.08	0	14.29	1.66	-2.71	0.47	0.18	[11]
G0	p	0.153	7.5	3.03	-2.73	0.09	0	15.27	1.89	-2.22	0.51	0.21	[11]
G0	p	0.164	7.77	3.03	-3.03	0.11	0	16.49	2.19	-2.88	0.54	0.23	[11]
G0	p	0.177	8.09	3.03	-3.41	0.13	0	17.93	2.58	-3.95	0.50	0.20	[11]
G0	p	0.192	8.43	3.03	-3.87	0.15	0	19.63	3.07	-3.85	0.53	0.19	[11]
G0	p	0.210	8.84	3.03	-4.45	0.19	0	21.69	3.72	-4.68	0.54	0.21	[11]
G0	p	0.232	9.31	3.03	-5.20	0.23	0	24.25	4.62	-5.27	0.59	0.23	[11]
G0	p	0.262	9.92	3.03	-6.29	0.31	0	27.82	6.03	-5.26	0.53	0.17	[11]
G0	p	0.299	10.63	3.03	-7.73	0.42	0	32.33	8.06	-7.72	0.80	0.35	[11]
G0	p	0.344	11.45	3.03	-9.61	0.58	0	37.97	11.01	-8.40	1.09	0.52	[11]
G0	p	0.410	12.59	3.03	-12.60	0.87	0	46.50	16.34	-10.25	1.11	0.55	[11]
G0	p	0.511	14.2	3.03	-17.61	1.49	0	60.11	27.01	-16.81	1.73	1.50	[11]
G0	p	0.631	15.98	3.03	-24.05	2.52	0	77.05	44.07	-19.96	1.69	1.31	[11]
G0	p	0.788	18.16	3.03	-33.08	4.45	0	100.26	74.55	-30.83	3.16	2.59	[11]
G0	p	0.997	20.9	3.03	-45.78	8.32	0	132.55	131.72	-37.93	11.55	0.52	[11]
HAPPEX	He ⁴	0.091	6.0	2.91	-7.52	0	0	-20.22	0	-6.72	0.87	0	[6]
HAPPEX	p	0.099	6.0	3.03	-1.41	0.04	0	9.54	0.76	-1.14	0.25	0	[8]
HAPPEX	He ⁴	0.077	6.0	2.67	-6.37	0	0	-16.58	0	-6.40	0.26	0	[9]
HAPPEX	p	0.109	6.0	3.18	-1.63	0.04	0	10.58	0.93	-1.58	0.13	0	[9]
PVA4	p	0.22	144.5	0.31	-13.31	3.47	0	2.88	11.13	-17.23	1.21	0	[4]
G0	p	0.221	110	0.35	-10.61	2.73	0	9.37	8.93	-11.25	0.9	0.43	[12]
G0	d	0.221	110	0.35	-15.25	2.05	-1.38	7.63	2.21	-16.93	0.91	0.21	[12]
G0	p	0.628	110	0.68	-36.91	11.91	0	19.71	62.25	-45.9	2.53	1.0	[12]
G0	d	0.628	110	0.68	-50.72	8.46	-5.66	16.63	14.62	-55.5	3.86	0.7	[12]
HAPPEX	p	0.624	13.7	3.48	-23.54	2.12	0	76.59	42.76	-23.8	0.86	0	[10]
PVA4	d	0.224	145	0.31	-18.65	2.50	-1.68	2.17	2.67	-20.11	1.35	0	[51]
Qweak	p	0.025	7.9	1.16	-0.22	0.006	0	2.27	0.05	-0.279	0.05	0	[18]

- [15] G. A. Miller, A. K. Oppen, and E. J. Stephenson, *Ann. Rev. Nucl. Part. Sci.* **56**, 253 (2006), arXiv:nucl-ex/0602021 [nucl-ex].
- [16] R. Lewis and N. Mobed, *Phys. Rev.* **D59**, 073002 (1999), arXiv:hep-ph/9810254 [hep-ph].
- [17] P. E. Shanahan, R. Horsley, Y. Nakamura, D. Pleiter, P. E. L. Rakow, G. Schierholz, H. Stuben, A. W. Thomas, R. D. Young, and J. M. Zanotti, *Phys. Rev.* **D91**, 113006 (2015), arXiv:1503.01142 [hep-lat].
- [18] D. Androic *et al.* (Qweak), *Phys. Rev. Lett.* **111**, 141803 (2013), arXiv:1307.5275 [nucl-ex].
- [19] D. H. Beck, *Phys. Rev.* **D39**, 3248 (1989).
- [20] R. D. Mckeown, *Phys. Lett.* **B219**, 140 (1989).
- [21] M. J. Musolf, T. W. Donnelly, J. Dubach, S. J. Pollock, S. Kowalski, and E. J. Beise, *Phys. Rept.* **239**, 1 (1994).
- [22] M. Tanabashi *et al.* (Particle Data Group), *Phys. Rev.* **D98**, 030001 (2018).
- [23] T. W. Donnelly, J. Dubach, and I. Sick, *Nucl. Phys.* **A503**, 589 (1989).
- [24] O. Moreno and T. W. Donnelly, *Phys. Rev.* **C89**, 015501 (2014), arXiv:1311.1843 [nucl-th].
- [25] R. D. Young, J. Roche, R. D. Carlini, and A. W. Thomas, *Phys. Rev. Lett.* **97**, 102002 (2006), arXiv:nucl-ex/0604010 [nucl-ex].
- [26] M. J. Musolf and B. R. Holstein, *Phys. Lett.* **B242**, 461 (1990).
- [27] W. J. Marciano and A. Sirlin, *Phys. Rev.* **D27**, 552 (1983).
- [28] M. Gorchtein and C. J. Horowitz, *Phys. Rev. Lett.* **102**, 091806 (2009), arXiv:0811.0614 [hep-ph].
- [29] D. Androic *et al.* (Qweak), *Nature* **557**, 207 (2018).
- [30] N. L. Hall, P. G. Blunden, W. Melnitchouk, A. W. Thomas, and R. D. Young, *Phys. Rev.* **D88**, 013011 (2013), arXiv:1304.7877 [nucl-th].
- [31] D. Wang *et al.* (PVDIS), *Nature* **506**, 67 (2014).
- [32] N. L. Hall, P. G. Blunden, W. Melnitchouk, A. W. Thomas, and R. D. Young, *Phys. Lett.* **B753**, 221 (2016), arXiv:1504.03973 [nucl-th].

TABLE IV. The $\square_{\gamma Z}(E)$ ($\times 10^{-3}$) corrections evaluated for the measured proton PV asymmetry A_{PV}^p at forward angles.

Experiment	Q^2 (GeV ²)	E (GeV)	$\square_{\gamma Z}(E)$ ($\times 10^{-3}$)
Qweak	0.025	1.165	5.120 ± 0.671
HAPPEX	0.099	3.030	7.205 ± 0.701
PVA4	0.108	0.570	2.843 ± 0.580
HAPPEX	0.109	3.180	7.250 ± 0.713
G0	0.122	3.030	6.969 ± 0.722
G0	0.128	3.030	6.907 ± 0.728
G0	0.136	3.030	6.825 ± 0.737
G0	0.144	3.030	6.742 ± 0.745
G0	0.153	3.030	6.648 ± 0.754
G0	0.164	3.030	6.534 ± 0.766
G0	0.177	3.030	6.398 ± 0.780
G0	0.192	3.030	6.243 ± 0.795
G0	0.210	3.030	6.056 ± 0.814
PVA4	0.230	0.850	3.257 ± 0.610
G0	0.232	3.030	5.831 ± 0.834
G0	0.262	3.030	5.527 ± 0.859
G0	0.299	3.030	5.161 ± 0.885
G0	0.344	3.030	4.733 ± 0.905
G0	0.410	3.030	4.143 ± 0.917
HAPPEX	0.477	3.350	3.749 ± 0.943
G0	0.511	3.030	3.340 ± 0.898
HAPPEX	0.624	3.480	2.740 ± 0.881
G0	0.631	3.030	2.547 ± 0.831
G0	0.788	3.030	1.753 ± 0.706
G0	0.997	3.030	1.038 ± 0.525

- [33] M. Gorchtein, C. J. Horowitz, and M. J. Ramsey-Musolf, Phys. Rev. **C84**, 015502 (2011), arXiv:1102.3910 [nucl-th].
- [34] Z. Ye, J. Arrington, R. J. Hill, and G. Lee, Phys. Lett. **B777**, 8 (2018), arXiv:1707.09063 [nucl-ex].
- [35] V. Bernard, L. Elouadrhiri, and U.-G. Meissner, J. Phys. **G28**, R1 (2002), arXiv:hep-ph/0107088 [hep-ph].
- [36] S.-L. Zhu, S. J. Puglia, B. R. Holstein, and M. J. Ramsey-Musolf, Phys. Rev. **D62**, 033008 (2000), arXiv:hep-ph/0002252 [hep-ph].
- [37] R. E. Cutkosky and B. B. Deo, Phys. Rev. **174**, 1859 (1968).
- [38] R. J. Hill and G. Paz, Phys. Rev. **D82**, 113005 (2010), arXiv:1008.4619 [hep-ph].
- [39] Z. Epstein, G. Paz, and J. Roy, Phys. Rev. **D90**, 074027 (2014), arXiv:1407.5683 [hep-ph].
- [40] R. González-Jiménez, J. A. Caballero, and T. W. Donnelly, Phys. Rev. **D90**, 033002 (2014), arXiv:1403.5119 [nucl-th].
- [41] R. D. Young, R. D. Carlini, A. W. Thomas, and J. Roche, Phys. Rev. Lett. **99**, 122003 (2007), arXiv:0704.2618 [hep-ph].
- [42] J. Liu, R. D. McKeown, and M. J. Ramsey-Musolf, Phys. Rev. **C76**, 025202 (2007), arXiv:0706.0226 [nucl-ex].
- [43] P. E. Shanahan, R. Horsley, Y. Nakamura, D. Pleiter, P. E. L. Rakow, G. Schierholz, H. Stüben, A. W. Thomas, R. D. Young, and J. M. Zanotti, Phys. Rev. Lett. **114**, 091802 (2015), arXiv:1403.6537 [hep-lat].
- [44] R. S. Sufian, Y.-B. Yang, A. Alexandru, T. Draper, J. Liang, and K.-F. Liu (χ QCD Collaboration), Phys. Rev. Lett. **118**, 042001 (2017).
- [45] J. Green, S. Meinel, M. Engelhardt, S. Krieg, J. Laeuchli, J. Negele, K. Orginos, A. Pochinsky, and S. Syritsyn, Phys. Rev. **D92**, 031501 (2015), arXiv:1505.01803 [hep-lat].
- [46] D. B. Leinweber, S. Boinapalli, I. C. Cloet, A. W. Thomas, A. G. Williams, R. D. Young, J. M. Zanotti, and J. B. Zhang, Phys. Rev. Lett. **94**, 212001 (2005), arXiv:hep-lat/0406002 [hep-lat].
- [47] D. B. Leinweber, S. Boinapalli, A. W. Thomas, P. Wang, A. G. Williams, R. D. Young, J. M. Zanotti, and J. B. Zhang, Phys. Rev. Lett. **97**, 022001 (2006), arXiv:hep-lat/0601025 [hep-lat].
- [48] P. Wang, D. B. Leinweber, A. W. Thomas, and R. D. Young, Phys. Rev. **C79**, 065202 (2009), arXiv:0807.0944 [hep-ph].
- [49] O. Moreno, T. W. Donnelly, R. González-Jiménez, and J. A. Caballero, J. Phys. **G42**, 034006 (2015), arXiv:1408.3511 [nucl-th].
- [50] M. Viviani, R. Schiavilla, B. Kubis, R. Lewis, L. Girlanda, A. Kievsky, L. E. Marcucci, and S. Rosati, Phys. Rev. Lett. **99**, 112002 (2007), arXiv:nucl-th/0703051 [NUCL-TH].
- [51] D. Balaguer Ríos *et al.*, Phys. Rev. **D94**, 051101 (2016).